Published in final edited form as:
Angiogenesis. 2010 June ; 13(2): 149–160. doi:10.1007/s10456-010-9167-z.

Non-invasive imaging of angiogenesis in head and neck squamous cell carcinoma

Jacobus F. A. Jansen[1,2], **Jason A. Koutcher**[1,2,3], and **Amita Shukla-Dave**[1,2]

Amita Shukla-Dave: davea@mskcc.org

[1] Department of Medical Physics, Memorial Sloan-Kettering Cancer Center, 1275 York Avenue, New York, NY 10065, USA

[2] Department of Radiology, Memorial Sloan-Kettering Cancer Center, New York, NY, USA

[3] Department of Medicine, Memorial Sloan-Kettering Cancer Center, New York, NY, USA

Abstract

Squamous cell carcinoma of the head and neck (HNSCC) is the seventh most common cancer in the United States. Angiogenesis, the process by which new blood vessels are formed, is an essential element at the basis of both tumor growth and metastases. This review discusses pertinent aspects of the role of imaging modalities in assessing angiogenesis and anti-angiogenic therapy in advanced HNSCC.

Keywords

Head and neck squamous cell carcinoma; Angiogenesis; Anti-angiogenic treatment; Imaging techniques; Magnetic resonance imaging; Computed tomography; Positron emission tomography; Ultrasound; Molecular imaging

Advanced head and neck cancers

In 2009, it was estimated that 48,010 new cases of head and neck (HN) cancer would be diagnosed in the United States and 11,260 deaths would occur due to the disease [1]. HN cancers generally stem from the mucosal epithelia of the oral cavity, pharynx, and larynx and have been etiologically associated with tobacco smoking and alcohol consumption [2]. Due to the wide variation in tissues of origin, HN cancer is a heterogeneous disease, representing a variety of histologies and differentiation patterns. The most common histology is squamous cell carcinoma (SCC), which accounts for greater than 90% of HN cancers. Early HN cancers are treated with radiation or surgery and have encouraging locoregional control [3,4]. After standard therapy (induction or concurrent chemotherapy administered with radiation or prior to surgery) for advanced HN disease, only 60% of patients survive 5 years [1]. Even with aggressive intervention, HN cancers often metastasize to the cervical lymph nodes before invading distant organs including the lungs. Despite advances in surgical techniques and oncologic treatment, the survival rate has remained the same over the past decade [1]. The two main reasons for poor outcome in advance HN cancer are a delayed diagnosis leading to locoregional failure and a late intervention with salvage treatment when disease recurs [5,6]. Therefore, even if the initial

Correspondence to: Amita Shukla-Dave, davea@mskcc.org.

carcinoma is successfully removed, the risk of a patient with HN cancer dying from this or a second malignancy remains high. This review will focus on advanced HNSCC.

Angiogenesis and therapy

Angiogenesis is a critical element of tumor growth and metastasis. It is a complex process, consisting of multiple steps concerning endothelial cell cessation, proliferation and migration of endothelial cells, and formation of new blood vessels [7]. During angiogenesis, vessels form to provide the expanding tumor with cells of endothelial origin, which divide much faster than normal endothelial cells. Once tumors grow beyond a diameter of a few millimeters, passive diffusion cannot sustain the viability of malignant cells anymore, and hence the formation of a new vascular network is necessary [7]. Tumors that grow beyond this stage, therefore, are capable of activating the “angiogenic switch.” Induction of this angiogenic switch depends on how heavily the balance tips in favor of angiogenesis. The induction can occur at different stages of tumor formation, depending on factors such as tumor type and the microenvironment. Blood vessel formation will persist as long as the tumor is growing and is aimed at feeding essential nutrients and oxygen to hypoxic and necrotic areas of the tumor. Angiogenesis plays an important role in head and neck squamous cell carcinoma (HNSCC) as in any other solid tumor [8]. The ability of the tumor to start angiogenesis is a prerequisite for metastatic spread. Traditionally, microvessel density (MVD) has been the parameter most often used for assessing angiogenesis [9]. Another approach involves the assessment of circulating angiogenic serum markers (e.g., vascular endothelial growth factor (VEGF)) [9].

Several studies [10–12] have shown that monitoring tumor angiogenesis has prognostic value. Angiogenesis is linked to an increased risk of local regional recurrence, distant metastases, and reduced survival in patients with cancers at various organs, including breast, lung, and ovary. Hence, angiogenesis is an interesting area of oncologic research. However, accurate means are needed for detecting tumor angiogenesis and monitoring treatment-induced changes in angiogenesis that precede changes in tumor size [7]. Promising developments in HNSCC angiogenesis research have engendered a need for a reliable pre-clinical platform to develop new therapies and validate surrogate markers of their efficacy in vivo [8].

The “gold-standard” MVD measure of angiogenesis is the histological estimate of the average number of micro-vessels within a selected region. Several studies have found that intratumoral MVD is predictive of outcome in a number of HNSCC disease sites and could aid the identification of patients who may need aggressive or adjuvant therapy [13–15]. However, the histological MVD assessment is inherently invasive and cannot clarify whether there are functional vessels with blood flow and whether vessels are of a hyperpermeable nature. Also, the assessment of serum marker VEGF lacks sufficient sensitivity and specificity [9].

Tumors are heterogeneous. Angiogenesis usually peaks in the tumor rim, and therefore MVD measures will fluctuate at different locations where the biopsy is obtained and may under- or over-estimate the degree of angiogenesis. Hence, the MVD parameter is more similar to a static “snap-shot” that does not lend itself to either dynamic in situ assessment of the tumor vasculature or of the molecular factors that regulate its growth [15]. Intratumoral MVD determination requires an invasive process with associated risks of hemorrhage and infection. Development of alternative, non-invasive methods for the evaluation of angiogenesis could spare patients from the aforementioned dangers [16].

Imaging

Imaging has many advantages as a means for improving the evaluation of angiogenesis, as it offers the ability to non-invasively sample the entire tumor, can be performed repetitively, and can be used to monitor changes in large numbers of patients at regular intervals [17]. The ability to accurately monitor angiogenesis response to therapy would allow drug efficacy to be established at a very early stage of treatment, long before traditional criteria, such as size changes, can be assessed; likewise, it would allow early identification of patients that do not response to treatment, so their treatment management plan can be altered. The modalities that have mainly been used for imaging angiogenesis include magnetic resonance imaging (MRI), computed tomography (CT), positron emission tomography (PET), and ultrasound (US).

Perfusion

Angiogenesis is typically heterogeneous within tumors: Some vessels are mature, whereas other vessels demonstrate incomplete layers with high permeability and fragility [7]. Angiogenic vessels have large gaps between the endothelial cells and the endothelium, making the vessels hyperpermeable to many macromolecules [18]. These properties can be exploited by imaging techniques that are aimed at assessing the leakiness of the tumor. The two most common modalities used for this purpose are CT perfusion (CTP) and dynamic contrast-enhanced MRI (DCE-MRI); both are well-established imaging techniques that can help assess physiologic parameters [18].

CTP

CTP provides the ability to quantify the microvascular blood flow of tissue by looking at dynamic scan series during injection enhancement of an iodine-based contrast agent [19]. As a clinical tool, CTP has been used mainly in evaluating intracranial vascular disorders such as stroke and vasospasm and to characterize intracranial masses and pathologic processes [20]. In oncology, it has been shown that the CTP parameters of blood flow (BF), blood volume (BV), mean transit time (MTT), and capillary permeability (CP) can be helpful in assessing tumors [21]. In HNSCC, BF, BV, and CP values have been reported to be elevated, and MTT values reduced relative to the values of these parameters in normal adjacent structures [22]. Additionally, Hermans et al. [23] demonstrated that perfusion assessed on CTP in HNSCC is an independent predictor of outcome after definitive radiation therapy with or without chemotherapy. Specifically, they reported that a lower pre-treatment (radiation) perfusion rate had a significantly higher local failure rate. Interestingly, Gandhi et al. [24] and Zima et al. [25] demonstrated that CT-determined BV before treatment or after induction chemotherapy correlated significantly with response in advanced HNSCC. High pre-treatment (induction chemotherapy) BV was linked to beneficial outcome; and a reduced BV post-treatment was linked to good response. Finally, Ash et al. [26] demonstrated that in HNSCC, the CTP-derived parameters BF and BV correlated positively with MVD as determined through histology, indicating the potential of CTP for assessing angiogenesis in vivo (Fig. 1).

DCE-MRI

In DCE-MRI, injection of the contrast agent gadopentetate dimeglumine (Gd-DTPA) intravenously is followed by the agent passing from the intravascular space to the interstitial space at a rate that depends on perfusion, vascularity, and tissue permeability [27]. In addition to above factors, the signal enhancement is also influenced by the leakage (interstitial) space. The contrast agent decreases the T1 (longitudinal relaxation time) value of blood and hence enhances the signal intensity on T1-weighted imaging. The blood signal

can be sampled by rapid serial T1-weighted imaging covering the tissue or organ of interest using intervals in the seconds range, for periods of up to several minutes after injection.

Using compartmental modeling, DCE-MR images can be converted into parameters reflecting tumor biology. The signal enhancement on T1-weighted images can be modeled using semi-quantitative or quantitative methods. Semi-quantitative methods can provide parameters like peak enhancement, maximum slope, and washout slope. Quantitative methods yield parameters such as K^{trans} (volume transfer constant in min^{-1}), v_e (volume fraction of the extravascular extracellular space which is dimensionless), and k_{ep} (rate constant in min^{-1}) [28]. Figure 2 displays a typical temporal resolution obtained in the pre-treatment DCE-MRI exam of a patient with HNSCC. This patient died of disease after initial treatment with surgery. The VEGF immunohistochemistry assay was performed on the surgical specimen (neck node metastases). More than 50% positive immunostaining for VEGF expression was observed in the nodal tissue.

So far, few studies have described the characteristic DCE-MRI enhancement patterns of tumors in the HN region. Konouchi et al. [29] have studied 30 patients with primary oral cavity and oropharyngeal SCC with DCE-MRI and correlated the findings with PCNA (proliferating cell nuclear antigen). The PCNA labeling index showed a significant correlation with maximum contrast index (CI) and maximum CI gain. Hoskin et al. [30] found in 13 patients with advanced HN cancer that tumors with diminished perfusion at the end of radiotherapy were those most sensitive to treatment and that tumors which showed greater enhancement after accelerated radiotherapy were likely to fail locally. Cao et al. [31] performed quantification of blood volume (BV) and blood flow (BF) from DCE-MRI data pre-therapy and 2 weeks after initiation of chemoradiation in 14 HNSCC patients with advanced disease; they showed that an increase in available primary tumor blood (i.e., BV) for oxygen extraction during RT was associated with increased local control. Finally, in a cohort of 33 patients with HNSCC with neck nodal metastases, Kim et al. [32] have shown that the average pre-treatment DCE-MRI parameter K^{trans} value was predictive of response to chemoradiation with a 6-month follow-up. Specifically, high pre-treatment perfusion (as measured by K^{trans}) was indicative of better treatment outcome.

Most HNSCC perfusion (CTP and DCE-MRI) studies so far report that high pre-treatment perfusion is linked to favorable treatment outcome [23–25,32] and that a large reduction in perfusion after treatment is also linked to better response [24,30]. Conflicting results, where an increase in BV after treatment is linked to favorable outcome, as reported by Cao et al. [31], have been tentatively been attributed to differences in treatment modalities, endpoints for local control, and data analyses methods [31]. Perfusion studies done with either CTP or DCE-MRI have shown their potential for monitoring treatment response in HNSCC. However, larger prospective trials are needed to confirm these findings.

DWI

Diffusion-weighted Imaging (DWI) is a technique that allows the non-invasive measurement of water diffusivity. It probes the structure and integrity of biological tissue at a microscopic level and may be used for in vivo tumor characterization [33]. Since freedom of translational motion of water molecules is hindered by interactions with other molecules and cellular barriers, such as membranes or different organelles, DWI abnormalities exhibit changes of tissue organization at the cellular level. These microstructural changes affect the (hindered) motion of water molecules and consequently alter the water diffusion properties and therefore the MRI signal. The signal loss in DWI can be quantified using the apparent diffusion coefficient (ADC), which can be interpreted as a measure of the average molecular motion that is affected by cellular organization.

In most DWI studies in patients with HN cancer, a combination of 2 or 3 b-factors was typically acquired, and the ADC values were calculated using the assumption that the signal intensity decay is of monoexponential origin [34–40]. Jansen et al. [41] recently showed the feasibility of non-Gaussian fitting by using the kurtosis model of the signal intensity decay curves obtained from performing DWI with an extended range of b-values in patients with HNSCC; the method they proposed yielded a significantly better fit of the data than did monoexponential modeling. The method also provided an additional parameter, K_{app}, which may provide added value. (Fig. 3).

The link between DWI findings and angiogenesis is not direct, but it has been hypothesized previously that tumors with a higher pre-treatment ADC are more susceptible to the effects of therapy with vascular disrupting or anti-angiogenesis agents [42]. In particular, Koh et al. [42] suggested, based on results of DWI in 15 patients with solid tumors (mostly colorectal and ovarian), that immature tumor vessels which predominate at the edge of necrotic regions (with high ADC values) are more susceptible to the anti-angiogenic agent bevacizumab. Another tentative link between angiogenesis and ADC was given by Liu et al. [43] in a preliminary report, who performed ADC, MVD, and VEGF measurements in 38 patients with prostate cancer. They observed a negative correlation between ADC values and MVD (and VEGF). This can be interpreted as higher cell density will result in restricted water motion (diffusion). However, these results need to be validated.

In HN cancers, mean ADC values have been mainly used to monitor treatment response, differentiate between benign and cancerous tissue, and to assess residual or recurrent tumors [34–40]. Wang et al. [35] studied 97 patients with HN at 1.5T and reported mean ADC values for lesions with different underlying pathologies. They showed that ADC values helped in characterizing HN lesions. Vandecaveye et al. [38] reported a study on four patients in which the mean ADC values of the lesions could be used to differentiate between persistent or recurrent tumor after radiotherapy for laryngeal squamous cell carcinoma and radiotherapy-induced tissue alterations. Recently, Dirix et al. [44] found that assessment of mean ADC values of regions of interest could yield important information about salivary gland function before and after therapy and holds promise for investigating radiation-induced xerostomia. In HNSCC, there is some evidence that DWI is useful for predicting and detecting early response to treatment. Kim et al. [45] have reported on the use of DWI for the prediction and detection of early response to chemoradiation treatment in 33 patients with HNSCC. It was shown that low pre-treatment ADC values correspond to better outcome and that an increase of ADC's after treatment was also favorable for response. Additionally, Galban et al. [46] showed that DWI could provide both prognostic and spatial information during non-surgical organ preservation therapy in HNSCC. The results reported in this study were in agreement with Kim et al. that increase in ADC values after treatment (chemoradiation) was linked to favorable outcome.

MRS

Magnetic resonance spectroscopy (MRS) is a technique which allows quantification of in vivo metabolite concentrations of tissue, thus offering a window onto cell metabolism [47]. MRS has been performed in HN cancers for both primary tumors and neck nodal metastases [48]. The metabolites most commonly studied with in vivo ^{1}H-MRS are total choline (tCho, a product of phospholipid metabolism that is composed mainly of free choline, phosphocholine, phosphatidylcholine, and glycerophosphocholine) and lactate (a product of glycolysis). There is not a direct one-to-one link between angiogenesis and metabolism seen on MRS. However, elevated levels of lactate may be observed during the process of aggressive tumor development accompanied by angiogenesis (the evolution of the microenvironment) [49]. Also, the rate of tumor cell proliferation has been linked to choline and metabolites seen with phosphorus (^{31}P) MRS [50,51].

Numerous investigators have found elevated total choline in tumors and it has been suggested that the elevated tCho peak reflects an increased cell proliferation rate [52]. The accumulation of lactate in tumors may be caused by both aerobic glycolysis (a common process in tumors) and by anaerobic glycolysis due to hypoxic conditions. Detection of lactate (a potential biomarker) in tumor tissues using non-invasive MR is difficult because of the presence of lipids, which typically have high co-resonating peaks. Hence, data acquisitions need to be tailored to observe this peak in vivo. In HN cancer, spectral editing techniques have been used to observe the lactate peak [53,54]. ^{31}P MRS can show a number of metabolites that may offer critical information about the tumor: nucleoside triphosphates (NTPs); phosphocreatine (PCr) (energy metabolism); inorganic phosphate (Pi, intracellular pHi); phosphocholine and phosphoethanolamine, jointly denoted as phosphomonoesters (PMEs, phospholipid precursors); and glycerol esters of phosphocholine and phosphoethanolamine (glycerophosphocholine and glycerophosphoethanolamine), collectively referred to as phosphodiesters (PDEs) (phospholipid catabolites). PME and PDE metabolites are elevated in tumors with high cell membrane turnover and are therefore markers of proliferation. In HN cancers, ^{1}H-MRS has been used mainly to differentiate between normal and primary tumors via the choline peak, while ^{31}P-MRS has been used to predict response via the PME/NTP ratio [51]. MRS is a tool to study cell membrane metabolism, pH, and tumor energy status that may find applications in monitoring anti-angiogenic therapies.

PET

Positron emission tomography (PET) is a highly sensitive non-invasive technology that is well suited for the visualization of changes in metabolism in cancer. Before PET imaging, radiolabeled tracers are injected in non-pharmacological tracer doses. Three-dimensional PET data can then be obtained and reconstructed to show the concentrations and locations of the radionuclide [55]. PET imaging, like MRS, offers a window into the tumor metabolism and microenvironment. ^{18}F-fluorodeoxyglucose (^{18}F-FDG) is the radiotracer most commonly used to image HN cancer [55]. ^{18}F-FDG uptake is proportional to tissue glucose consumption. Most tumors have an elevated glucose consumption which can be quantified by ^{18}F-FDG PET imaging. This tracer has applications ranging from staging to prediction of outcome in HN cancers [55].

Many other PET tracers have been used to better understand the tumor microenvironment, especially angiogenesis, and related processes such as hypoxia and proliferation. The radiotracer ^{18}F-Galacto RGD has been developed for PET imaging of $\alpha v\beta 3$ expression of a receptor involved in angiogenesis and metastases [56]. Beer et al. [57] tested the feasibility of using this tracer in eleven patients with HNSCC. They performed immunohistochemistry (IHC) using an $\alpha v\beta 3$-specific antibody and expression of the antibody was seen in all cases. ^{18}F-Galacto RGD PET identified 10 of the 12 tumors correctly, and two tumors of size <0.5 mm were missed. They established the feasibility of using this tracer to open up new possibilities for studying angiogenesis with PET. An important application of this new radiotracer would be in monitoring treatment response of anti-angiogenic therapy.

^{18}F-fluoromisonidazole (FMISO) PET has been used to study hypoxia [58,59]. Hypoxia is a pathological condition in which tissue is deprived of adequate oxygen supply. Numerous investigators have stated that tumor oxygenation (using invasive Eppendorf pO2 measurements) in HN cancers is linked to poor outcome [60,61]. Nordsmark et al. [61] assessed the pre-treatment tumor oxygen tension in a multicentric trial with 397 patients with HN cancer and concluded that tumor hypoxia is associated with a poor outcome. ^{18}F-FMISO PET is only susceptible to hypoxia in viable cells; it can cover large regions of interest and is well tolerated by patients. Jansen et al. [62] showed that ^{18}F-FMISO PET hypoxia data correlated with DCE-MRI perfusion data in patients with HNSCC. They found

that in metastatic neck lymph nodes, hypoxic nodes were poorly perfused relative to those that were non-hypoxic (Fig. 4).

Another tracer that has been used in HN cancer is ^{18}F-fluorothymidine (^{18}F-FLT), the uptake of which reflects proliferation [63]. Cellular proliferation, or cell growth, is a major feature of cancer, in which cells exhibit uncontrolled growth and division at a larger rate than normal. This tracer is captured in proliferating tissues through the activity of thymidine kinase. ^{18}F-FLT uptake has been shown to be a marker of thymidine kinase-1 (TK1) activity, which is an enzyme that is overexpressed during the DNA synthesis phase of the cell cycle. Accumulation of ^{18}F-FLT inside the cell is, therefore, interpreted as a putative marker of proliferation. Few studies have used this tracer in primary HN cancers. Cobben et al. [64] showed in a prospective ^{18}F-FLT and ^{18}F-FDG PET study performed on 21 patients with suspected recurrent and primary laryngeal cancer that both techniques detected histologically proven laryngeal cancer correctly in 15 of 17 patients. Linecker et al. [65] took a step further and correlated ^{18}F-FLT data with the proliferative molecular marker Ki-67 assessed by IHC assay. They studied 20 untreated patients with HNCC by both ^{18}F-FLT and ^{18}F-FDG PET and compared the PET results with histological and IHC results. They found a significant inverse correlation between both ^{18}F-FLT uptake and survival but no correlation between Ki-67 expression level and ^{18}F-FLT PET data (which could be attributed to the small patient population). As seen by these studies, it is clear that PET tracers are being continuously tested for various applications in HN cancers and their role in better understanding the tumor microenvironment is still evolving. Mostly they have been used for detection and staging of the disease [55]. Going forward, roles for these tracers in monitoring anti-angiogenic therapy are expected to unfold.

US

Ultrasound offers an inexpensive and readily accessible means to evaluate cervical adenopathy, and it is the standard tool used for this purpose in the clinic [66]. Typically, clinical examinations are performed with a high-frequency, linear transducer, usually with Doppler capability. Substitution of neoplastic tissue for normal lymph node tissue makes lymph nodes unusually clear on ultrasonic examination. The complex, multi-step process of angiogenesis is critically associated with blood flow and blood flow regulation. It has been hypothesized that laser Doppler ultrasound could provide a non-invasive and reliable method of quantifying blood flow within tumors [67]. Jacob et al. [67] showed that laser Doppler ultrasound is a potentially useful tool for studying blood flow in the HN region.

Molecular imaging

Molecular imaging (MI) has been defined as the in vivo visual representation, characterization, and quantification of biologic processes and molecular pathways at a cellular and molecular level [68]. As long as a suitable target, probe, and detection method are available, the MI concept can be applied to various imaging modalities, including MR, CT, PET, US, and optical imaging. MI is rapidly gaining acceptance in oncology, as it detects differences in molecular properties in vivo between cancer and normal tissue that arise as a result of malignant transformation [69]. The above mentioned ^{18}F-Galacto RGD PET approach using the $\alpha v\beta 3$-specific antibody is an excellent example of MI use in angiogenesis [56]. Receptors play a key role in signal transduction and proliferation of cancer cells [70]. Another example of such a receptor is the transferrin receptor (TfR), which is a cell membrane-internalizing receptor that is responsible for iron sequestration in mammalian cells [71]. Expression of TfR is elevated in malignant cells due to a need for iron as a cofactor for the ribonucleotide reductase enzyme [71]. TfR is overexpressed in the majority of cases of HNSCC but minimally expressed in normal oral squamous epithelium and benign lesions [72]. A high expression level of TfR indicates a high grade of tumor

malignancy and a poor prognosis. TfR expression can be targeted in vivo by conjugating a transferrin (Tf) probe to a nanoparticle suited for MI, as shown elegantly by Shan et al. [73] in an animal model of HNSCC.

In addition to the two aforementioned MI approaches in HNSCC (TfR and $\alpha v\beta 3$), many other angiogenesis-related receptors can be targeted using MI. As new molecular therapies are by definition directed at specific targets, MI directed at the same targets can be useful in predicting the response to anti-angiogenic drug treatment. Such a targeted approach depends on the binding of labeled molecules to highly expressed markers. Interestingly, nanoparticles used for MI of angiogenesis may be designed such to have both diagnostic and anti-tumor features. This allow investigators to precisely monitor drug delivery and efficacy in tumors (theranostics) [74]. Molecules that are possible targets for imaging include VEGF and its receptors, integrins, and matrix metalloproteinases (MMPs) [17]. The application of MI of angiogenesis in HNSCC has been very limited so far, therefore we would like to refer to articles by Turkbey et al. [17] and Cai et al. [75] who provide excellent, more extensive reviews of potential targets for MI of angiogenesis.

Imaging of angiogenesis-targeted therapy in HNSCC

Current HNSCC treatment protocols for advanced disease include aggressive induction chemotherapy and concurrent chemoradiation, with an increasing role for novel, rationally designed, molecularly targeted agents [76]. There is a growing need for additional clinical diagnostic tests to help select treatments with maximal efficacy and minimal toxicity [8]. Unlike cytotoxic chemotherapy, which interrupts normal mitotic activity in dividing cells, targeted therapies are designed to interact primarily with cancer-specific attributes and signaling pathways [8]. One of these pathways is angiogenesis, a characteristic of all advanced cancers.

Pre-clinical and early clinical trials provide evidence of the promise of anti-angiogenic therapy for HNSCC [8]. Seiwert et al. [8] recently provided an overview of the currently available data and future directions for treatment, including ongoing pivotal clinical trials. Contrary to earlier fears that anti-angiogenic therapies could augment hypoxia and thereby might make treatment failure more likely, anti-angiogenic therapies in pre-clinical HNSCC models so far do not appear to have a propensity for resistance and go well with traditional therapies (such as radiation).

Clinical use of anti-angiogenic agents for HNSCC often focus on inhibitors of tyrosine kinase receptors, including bevacizumab, sorafenib, sunitinib, semaxanib, and others. Their use is currently limited to clinical trials, and therefore, literature on the use of imaging to monitor angiogenesis in HNSCC patients treated with anti-angiogenic drugs is scarce. It is pertinent to point out that most of the aforementioned studies of the use of imaging techniques to monitor treatment in HNSCC did not pertain to anti-angiogenic drugs, but to radiation or cytotoxic chemotherapy [8]. In a recent Phase II study by Machiels et al. [77], 38 patients with HNSCC were treated with sunitinib and a small subset of patients underwent DCE-MRI monitoring pre- and post-treatment. The DCE-MRI results showed that in all but one of the patients studied, a significant decrease was observed in K^{trans} after treatment, suggesting that sunitinib indeed decreased the amount of angiogenesis. In another Phase II study, Fury et al. [78] used power Doppler ultrasound and serum VEGF levels to monitor anti-angiogenic activity of semaxanib in 35 patients with HNSCC. They found that tumor vascularity decreased during semaxanib treatment even in patient with progression of disease. They concluded that semaxanib achieved suboptimal inhibition of angiogenesis and that changes observed with ultrasound were probably not related to anti-tumor activity of semaxanib. These Phase II feasibility studies indicate the need for reliable imaging

techniques to monitor angiogenesis (or angiogenesis-related processes) in HNSCC trials of anti-angiogenic agents.

The ability to detect diverse aspects of angiogenesis and angiogenesis-related processes makes in vivo imaging attractive for following the entire time course of drugs' anti-angiogenic activity in HNSCC. Anti-angiogenic agents target tumor vasculature and reduce vessel permeability by 'normalizing' the vessel morphology, which restores vascular integrity [79]. Clinically, imaging can be applied before, during, and after anti-angiogenic treatment to monitor response. A comprehensive overview of the presented imaging techniques and their relation to angiogenesis is provided in Fig. 5 and Table 1.

Do we really image angiogenesis?

As indicated above, most imaging modalities, with the exception of ^{18}F-Galacto RGD PET, do not provide direct information about angiogenesis itself, but merely about a related process. Therefore, the exact relevance of the changes observed in tissue contrast (as measured using one of the imaging modalities) to angiogenesis remains speculative in nature. However, sufficient evidence is available showing that techniques as CTP [26], DCE-MRI [80], and US [81] closely correlate with MVD measurements, which can be regarded as a gold-standard. Unfortunately, for other techniques, a similar validation with MVD is not conclusive (DWI [43], FDG PET [82], and FMISO PET [83]) or lacks completely (MRS and FLT PET). Another relevant issue for all techniques used for imaging angiogenesis or angiogenesis-related processes is the proper analysis (e.g. modeling) of the data and the reproducibility of the imaging measurements. These are prerequisites in order to objectively infer whether measured changes in imaging parameters truly reflect the biological process.

Conclusion

Considering the diversity and demonstrated potential of available imaging methods, the importance of imaging in assessing angiogenesis in HNSCC is expected to grow.

Acknowledgments

We thank Ms. Ada Muellner (B.A.) for editing the manuscript and Dr Diane Carlson (Dept of Pathology) for molecular pathology data on surgical specimens. The work from MSKCC reported in this review was supported by the National Cancer Institute/National Institutes of Health (grant number 1 R01 CA115895).

References

1. Jemal A, Siegel R, Ward E, Hao Y, Xu J, Thun MJ. Cancer statistics. CA Cancer J Clin 2009;59:225–249. [PubMed: 19474385]
2. Vokes EE, Weichselbaum RR, Lippman SM, Hong WK. Head and neck cancer. N Engl J Med 1993;328:184–194. [PubMed: 8417385]
3. Klem ML, Mechalakos JG, Wolden SL, Zelefsky MJ, Singh B, Kraus D, Shaha A, Shah J, Pfister DG, Lee NY. Intensity-modulated radiotherapy for head and neck cancer of unknown primary: toxicity and preliminary efficacy. Int J Radiat Oncol Biol Phys 2008;70:1100–1107. [PubMed: 17980501]
4. Lee NY, O'Meara W, Chan K, Della-Bianca C, Mechalakos JG, Zhung J, Wolden SL, Narayana A, Kraus D, Shah JP, Pfister DG. Concurrent chemotherapy and intensity-modulated radiotherapy for locoregionally advanced laryngeal and hypo-pharyngeal cancers. Int J Radiat Oncol Biol Phys 2007;69:459–468. [PubMed: 17493769]
5. Schwartz LH, Ozsahin M, Zhang GN, Touboul E, De Vataire F, Andolenko P, Lacau-Saint-Guily J, Laugier A, Schlienger M. Synchronous and metachronous head and neck carcinomas. Cancer 1994;74:1933–1938. [PubMed: 8082099]

6. Day GL, Blot WJ. Second primary tumors in patients with oral cancer. Cancer 1992;70:14–19. [PubMed: 1606536]
7. Carmeliet P, Jain RK. Angiogenesis in cancer and other diseases. Nature 2000;407:249–257. [PubMed: 11001068]
8. Seiwert TY, Cohen EE. Targeting angiogenesis in head and neck cancer. Semin Oncol 2008;35:274–285. [PubMed: 18544442]
9. Palka KT, Slebos RJ, Chung CH. Update on molecular diagnostic tests in head and neck cancer. Semin Oncol 2008;35:198–210. [PubMed: 18544435]
10. Weidner N, Folkman J, Pozza F, Bevilacqua P, Allred EN, Moore DH, Meli S, Gasparini G. Tumor angiogenesis: a new significant and independent prognostic indicator in early-stage breast carcinoma. J Natl Cancer Inst 1992;84:1875–1887. [PubMed: 1281237]
11. Mendiola M, Barriuso J, Redondo A, Marino-Enriquez A, Madero R, Espinosa E, Vara JA, Sanchez-Navarro I, Hernandez-Cortes G, Zamora P, Perez-Fernandez E, Miguel-Martin M, Suarez A, Palacios J, Gonzalez-Baron M, Hardisson D. Angiogenesis-related gene expression profile with independent prognostic value in advanced ovarian carcinoma. PLoS One 2008;3:e4051. [PubMed: 19112514]
12. Angeletti CA, Lucchi M, Fontanini G, Mussi A, Chella A, Ribechini A, Vignati S, Bevilacqua G. Prognostic significance of tumoral angiogenesis in completely resected late stage lung carcinoma (stage IIIA-N2). Impact of adjuvant therapies in a subset of patients at high risk of recurrence. Cancer 1996;78:409–415. [PubMed: 8697384]
13. Ito Y, Kamijo T, Yokose T, Kawashima M, Ogino T, Ikeda H, Hayashi R, Sasaki S, Ochiai A. Microvessel density predicts the radiosensitivity of metastatic head and neck squamous cell carcinoma in cervical lymph nodes. Int J Oncol 2001;19:1127–1132. [PubMed: 11713580]
14. Sauter ER, Nesbit M, Watson JC, Klein-Szanto A, Litwin S, Herlyn M. Vascular endothelial growth factor is a marker of tumor invasion and metastasis in squamous cell carcinomas of the head and neck. Clin Cancer Res 1999;5:775–782. [PubMed: 10213212]
15. Pignataro L, Carboni N, Midolo V, Bertolini F, Buffa R, Cesana BM, Neri A, Viale G, Pruneri G. Clinical relevance of microvessel density in laryngeal squamous cell carcinomas. Int J Cancer 2001;92:666–670. [PubMed: 11340569]
16. Jain RK, Duda DG, Willett CG, Sahani DV, Zhu AX, Loeffler JS, Batchelor TT, Sorensen AG. Biomarkers of response and resistance to antiangiogenic therapy. Nat Rev Clin Oncol 2009;6:327–338. [PubMed: 19483739]
17. Turkbey B, Kobayashi H, Ogawa M, Bernardo M, Choyke PL. Imaging of tumor angiogenesis: functional or targeted? AJR Am J Roentgenol 2009;193:304–313. [PubMed: 19620425]
18. Charnley N, Donaldson S, Price P. Imaging angiogenesis. Methods Mol Biol 2009;467:25–51. [PubMed: 19301663]
19. Faggioni L, Neri E, Bartolozzi C. CT perfusion of head and neck tumors: how we do it. AJR Am J Roentgenol 2010;194:62–69. [PubMed: 20028906]
20. Aksoy FG, Lev MH. Dynamic contrast-enhanced brain perfusion imaging: technique and clinical applications. Semin Ultrasound CT MR 2000;21:462–477. [PubMed: 11138635]
21. Shah GV, Wesolowski JR, Ansari SA, Mukherji SK. New directions in head and neck imaging. J Surg Oncol 2008;97:644–648. [PubMed: 18493943]
22. Gandhi D, Hoeffner EG, Carlos RC, Case I, Mukherji SK. Computed tomography perfusion of squamous cell carcinoma of the upper aerodigestive tract. Initial results. J Comput Assist Tomogr 2003;27:687–693. [PubMed: 14501359]
23. Hermans R, Meijerink M, Van den Bogaert W, Rijnders A, Weltens C, Lambin P. Tumor perfusion rate determined noninvasively by dynamic computed tomography predicts outcome in head-and-neck cancer after radiotherapy. Int J Radiat Oncol Biol Phys 2003;57:1351–1356. [PubMed: 14630273]
24. Gandhi D, Chepeha DB, Miller T, Carlos RC, Bradford CR, Karamchandani R, Worden F, Eisbruch A, Teknos TN, Wolf GT, Mukherji SK. Correlation between initial and early follow-up CT perfusion parameters with endoscopic tumor response in patients with advanced squamous cell carcinomas of the oropharynx treated with organ-preservation therapy. AJNR Am J Neuroradiol 2006;27:101–106. [PubMed: 16418366]

25. Zima A, Carlos R, Gandhi D, Case I, Teknos T, Mukherji SK. Can pretreatment CT perfusion predict response of advanced squamous cell carcinoma of the upper aerodigestive tract treated with induction chemotherapy? AJNR Am J Neuroradiol 2007;28:328–334. [PubMed: 17297007]
26. Ash L, Teknos TN, Gandhi D, Patel S, Mukherji SK. Head and neck squamous cell carcinoma: CT perfusion can help non-invasively predict intratumoral microvessel density. Radiology 2009;251:422–428. [PubMed: 19276321]
27. Hylton N. Dynamic contrast-enhanced magnetic resonance imaging as an imaging biomarker. J Clin Oncol 2006;24:3293–3298. [PubMed: 16829653]
28. Yankeelov TE, Gore JC. Dynamic contrast enhanced magnetic resonance imaging in oncology: theory, data acquisition, analysis and examples. Curr Med Imaging Rev 2007;3:91–107. [PubMed: 19829742]
29. Konouchi H, Asaumi J, Yanagi Y, Shigehara H, Hisatomi M, Matsuzaki H, Kishi K. Evaluation of tumor proliferation using dynamic contrast enhanced-MRI of oral cavity and oropharyngeal squamous cell carcinoma. Oral Oncol 2003;39:290–295. [PubMed: 12618202]
30. Hoskin PJ, Saunders MI, Goodchild K, Powell ME, Taylor NJ, Baddeley H. Dynamic contrast enhanced magnetic resonance scanning as a predictor of response to accelerated radiotherapy for advanced head and neck cancer. Br J Radiol 1999;72:1093–1098. [PubMed: 10700827]
31. Cao Y, Popovtzer A, Li D, Chepeha DB, Moyer JS, Prince ME, Worden F, Teknos T, Bradford C, Mukherji SK, Eisbruch A. Early prediction of outcome in advanced head-and-neck cancer based on tumor blood volume alterations during therapy: a prospective study. Int J Radiat Oncol Biol Phys 2008;72:1287–1290. [PubMed: 19028268]
32. Kim S, Loevner LA, Quon H, Kilger A, Sherman E, Weinstein G, Chalian A, Poptani H. Prediction of response to chemoradiation therapy in squamous cell carcinomas of the head and neck using dynamic contrast-enhanced MR imaging. AJNR Am J Neuroradiol 2010;31:262–268. [PubMed: 19797785]
33. Koh DM, Collins DJ. Diffusion-weighted MRI in the body: applications and challenges in oncology. AJR Am J Roentgenol 2007;188:1622–1635. [PubMed: 17515386]
34. Abdel Razek AA, Gaballa G, Elhawarey G, Megahed AS, Hafez M, Nada N. Characterization of pediatric head and neck masses with diffusion-weighted MR imaging. Eur Radiol 2009;19:201–208. [PubMed: 18704436]
35. Wang J, Takashima S, Takayama F, Kawakami S, Saito A, Matsushita T, Momose M, Ishiyama T. Head and neck lesions: characterization with diffusion-weighted echo-planar MR imaging. Radiology 2001;220:621–630. [PubMed: 11526259]
36. Sumi M, Nakamura T. Diagnostic importance of focal defects in the apparent diffusion coefficient-based differentiation between lymphoma and squamous cell carcinoma nodes in the neck. Eur Radiol 2009;19:975–981. [PubMed: 18958472]
37. Abdel Razek AA, Megahed AS, Denewer A, Motamed A, Tawfik A, Nada N. Role of diffusion-weighted magnetic resonance imaging in differentiation between the viable and necrotic parts of head and neck tumors. Acta Radiol 2008;49:364–370. [PubMed: 18365828]
38. Vandecaveye V, de Keyzer F, Vander Poorten V, Deraedt K, Alaerts H, Landuyt W, Nuyts S, Hermans R. Evaluation of the larynx for tumour recurrence by diffusion-weighted MRI after radiotherapy: initial experience in four cases. Br J Radiol 2006;79:681–687. [PubMed: 16641411]
39. Maeda M, Kato H, Sakuma H, Maier SE, Takeda K. Usefulness of the apparent diffusion coefficient in line scan diffusion-weighted imaging for distinguishing between squamous cell carcinomas and malignant lymphomas of the head and neck. AJNR Am J Neuroradiol 2005;26:1186–1192. [PubMed: 15891182]
40. Srinivasan A, Dvorak R, Perni K, Rohrer S, Mukherji SK. Differentiation of benign and malignant pathology in the head and neck using 3T apparent diffusion coefficient values: early experience. AJNR Am J Neuroradiol 2008;29:40–44. [PubMed: 17921228]
41. Jansen JF, Stambuk HE, Koutcher JA, Shukla-Dave A. Non-Gaussian analysis of diffusion-weighted MR imaging in head and neck squamous cell carcinoma: a feasibility study. AJNR Am J Neuroradiol. 200910.3174/ajnr.A1919
42. Koh DM, Blackledge M, Collins DJ, Padhani AR, Wallace T, Wilton B, Taylor NJ, Stirling JJ, Sinha R, Walicke P, Leach MO, Judson I, Nathan P. Reproducibility and changes in the apparent

diffusion coefficients of solid tumours treated with combretastatin A4 phosphate and bevacizumab in a two-centre phase I clinical trial. Eur Radiol 2009;19:2728–2738. [PubMed: 19547986]

43. Liu JG, Wang B, Wang XZ, Niu QL, Zhang Q. Diffusion weighted MRI helps evaluate angiogenesis and vascular endothelial growth factor expression in prostate cancer. Zhonghua Nan Ke Xue 2009;15:403–408. [PubMed: 19514550]
44. Dirix P, De Keyzer F, Vandecaveye V, Stroobants S, Hermans R, Nuyts S. Diffusion-weighted magnetic resonance imaging to evaluate major salivary gland function before and after radiotherapy. Int J Radiat Oncol Biol Phys 2008;71:1365–1371. [PubMed: 18355977]
45. Kim S, Loevner L, Quon H, Sherman E, Weinstein G, Kilger A, Poptani H. Diffusion-weighted magnetic resonance imaging for predicting and detecting early response to chemoradiation therapy of squamous cell carcinomas of the head and neck. Clin Cancer Res 2009;15:986–994. [PubMed: 19188170]
46. Galban CJ, Mukherji SK, Chenevert TL, Meyer CR, Hamstra DA, Bland PH, Johnson TD, Moffat BA, Rehemtulla A, Eisbruch A, Ross BD. A feasibility study of parametric response map analysis of diffusion-weighted magnetic resonance imaging scans of head and neck cancer patients for providing early detection of therapeutic efficacy. Transl Oncol 2009;2:184–190. [PubMed: 19701503]
47. Jansen JF, Backes WH, Nicolay K, Kooi ME. 1H MR spectroscopy of the brain: absolute quantification of metabolites. Radiology 2006;240:318–332. [PubMed: 16864664]
48. Shah GV, Gandhi D, Mukherji SK. Magnetic resonance spectroscopy of head and neck neoplasms. Top Magn Reson Imaging 2004;15:87–94. [PubMed: 15269611]
49. Thakur SB, Yaligar J, Koutcher JA. In vivo lactate signal enhancement using binomial spectral-selective pulses in selective MQ coherence (SS-SelMQC) spectroscopy. Magn Reson Med 2009;62:591–598. [PubMed: 19526486]
50. Chawla S, Kim S, Loevner LA, Quon H, Wang S, Mutale F, Weinstein G, Delikatny EJ, Poptani H. Proton and phosphorous MR spectroscopy in squamous cell carcinomas of the head and neck. Acad Radiol 2009;16:1366–1372. [PubMed: 19608433]
51. Shukla-Dave A, Poptani H, Loevner LA, Mancuso A, Serrai H, Rosenthal DI, Kilger AM, Nelson DS, Zakian KL, Arias-Mendoza F, Rijpkema M, Koutcher JA, Brown TR, Heerschap A, Glickson JD. Prediction of treatment response of head and neck cancers with P-31 MR spectroscopy from pretreatment relative phosphomonoester levels. Acad Radiol 2002;9:688–694. [PubMed: 12061743]
52. Aboagye EO, Bhujwalla ZM. Malignant transformation alters membrane choline phospholipid metabolism of human mammary epithelial cells. Cancer Res 1999;59:80–84. [PubMed: 9892190]
53. Star-Lack J, Spielman D, Adalsteinsson E, Kurhanewicz J, Terris DJ, Vigneron DB. In vivo lactate editing with simultaneous detection of choline, creatine, NAA, and lipid singlets at 1.5 T using PRESS excitation with applications to the study of brain and head and neck tumors. J Magn Reson 1998;133:243–254. [PubMed: 9716465]
54. Star-Lack JM, Adalsteinsson E, Adam MF, Terris DJ, Pinto HA, Brown JM, Spielman DM. In vivo 1H MR spectroscopy of human head and neck lymph node metastasis and comparison with oxygen tension measurements. AJNR Am J Neuroradiol 2000;21:183–193. [PubMed: 10669248]
55. Schoder H, Fury M, Lee N, Kraus D. PET monitoring of therapy response in head and neck squamous cell carcinoma. J Nucl Med 2009;50(Suppl 1):74S–88S. [PubMed: 19380408]
56. Beer AJ, Haubner R, Wolf I, Goebel M, Luderschmidt S, Niemeyer M, Grosu AL, Martinez MJ, Wester HJ, Weber WA, Schwaiger M. PET-based human dosimetry of 18F-galacto-RGD, a new radiotracer for imaging alpha v beta3 expression. J Nucl Med 2006;47:763–769. [PubMed: 16644745]
57. Beer AJ, Grosu AL, Carlsen J, Kolk A, Sarbia M, Stangier I, Watzlowik P, Wester HJ, Haubner R, Schwaiger M. [18F]galacto-RGD positron emission tomography for imaging of alphavbeta3 expression on the neovasculature in patients with squamous cell carcinoma of the head and neck. Clin Cancer Res 2007;13:6610–6616. [PubMed: 18006761]
58. Lee NY, Mechalakos JG, Nehmeh S, Lin Z, Squire OD, Cai S, Chan K, Zanzonico PB, Greco C, Ling CC, Humm JL, Schoder H. Fluorine-18-labeled fluoromisonidazole positron emission and

computed tomography-guided intensity-modulated radiotherapy for head and neck cancer: a feasibility study. Int J Radiat Oncol Biol Phys 2008;70:2–13. [PubMed: 17869020]

59. Rasey JS, Koh WJ, Evans ML, Peterson LM, Lewellen TK, Graham MM, Krohn KA. Quantifying regional hypoxia in human tumors with positron emission tomography of [18F]fluoromisonidazole: a pretherapy study of 37 patients. Int J Radiat Oncol Biol Phys 1996;36:417–428. [PubMed: 8892467]
60. Brizel DM, Dodge RK, Clough RW, Dewhirst MW. Oxygenation of head and neck cancer: changes during radiotherapy and impact on treatment outcome. Radiother Oncol 1999;53:113–117. [PubMed: 10665787]
61. Nordsmark M, Bentzen SM, Rudat V, Brizel D, Lartigau E, Stadler P, Becker A, Adam M, Molls M, Dunst J, Terris DJ, Overgaard J. Prognostic value of tumor oxygenation in 397 head and neck tumors after primary radiation therapy. An international multi-center study. Radiother Oncol 2005;77:18–24. [PubMed: 16098619]
62. Jansen JF, Schöder H, Lee NY, Wang Y, Pfister DG, Fury MG, Stambuk HE, Humm JL, Koutcher JA, Shukla-Dave A. Noninvasive assessment of tumor microenvironment using dynamic contrast-enhanced magnetic resonance imaging and (18)F-fluoromisonidazole positron emission tomography imaging in neck nodal metastases. Int J Radiat Oncol Biol Phys. 200910.1016/j.ijrobp.2009.07.009
63. Barthel H, Cleij MC, Collingridge DR, Hutchinson OC, Osman S, He Q, Luthra SK, Brady F, Price PM, Aboagye EO. 3′-deoxy-3′-[18F]fluorothymidine as a new marker for monitoring tumor response to antiproliferative therapy in vivo with positron emission tomography. Cancer Res 2003;63:3791–3798. [PubMed: 12839975]
64. Cobben DC, van der Laan BF, Maas B, Vaalburg W, Suurmeijer AJ, Hoekstra HJ, Jager PL, Elsinga PH. 18F-FLT PET for visualization of laryngeal cancer: comparison with 18F-FDG PET. J Nucl Med 2004;45:226–231. [PubMed: 14960640]
65. Linecker A, Kermer C, Sulzbacher I, Angelberger P, Kletter K, Dudczak R, Ewers R, Becherer A. Uptake of (18)F-FLT and (18)F-FDG in primary head and neck cancer correlates with survival. Nuklearmedizin 2008;47:80–85. (quiz N12). [PubMed: 18392317]
66. Richards PS, Peacock TE. The role of ultrasound in the detection of cervical lymph node metastases in clinically N0 squamous cell carcinoma of the head and neck. Cancer Imaging 2007;7:167–178. [PubMed: 18055290]
67. Jacob A, Varghese BE, Birchall MB. Validation of laser Doppler fluxmetry as a method of assessing neo-angiogenesis in laryngeal tumours. Eur Arch Otorhinolaryngol 2006;263:444–448. [PubMed: 16311774]
68. Massoud TF, Gambhir SS. Molecular imaging in living subjects: seeing fundamental biological processes in a new light. Genes Dev 2003;17:545–580. [PubMed: 12629038]
69. Weissleder R, Mahmood U. Molecular imaging. Radiology 2001;219:316–333. [PubMed: 11323453]
70. Winnard P Jr, Raman V. Real time non-invasive imaging of receptor-ligand interactions in vivo. J Cell Biochem 2003;90:454–463. [PubMed: 14523979]
71. Daniels TR, Delgado T, Helguera G, Penichet ML. The transferrin receptor part II: targeted delivery of therapeutic agents into cancer cells. Clin Immunol 2006;121:159–176. [PubMed: 16920030]
72. Kearsley JH, Furlong KL, Cooke RA, Waters MJ. An immunohistochemical assessment of cellular proliferation markers in head and neck squamous cell cancers. Br J Cancer 1990;61:821–827. [PubMed: 2372483]
73. Shan L, Hao Y, Wang S, Korotcov A, Zhang R, Wang T, Califano J, Gu X, Sridhar R, Bhujwalla ZM, Wang PC. Visualizing head and neck tumors in vivo using near-infrared fluorescent transferrin conjugate. Mol Imaging 2008;7:42–49. [PubMed: 18384723]
74. Liu Y, Miyoshi H, Nakamura M. Nanomedicine for drug delivery and imaging: a promising avenue for cancer therapy and diagnosis using targeted functional nanoparticles. Int J Cancer 2007;120:2527–2537. [PubMed: 17390371]
75. Cai W, Chen X. Multimodality molecular imaging of tumor angiogenesis. J Nucl Med 2008;49(Suppl 2):113S–128S. [PubMed: 18523069]

76. Cognetti DM, Weber RS, Lai SY. Head and neck cancer: an evolving treatment paradigm. Cancer 2008;113:1911–1932. [PubMed: 18798532]
77. Machiels JP, Henry S, Zanetta S, Kaminsky MC, Michoux N, Rommel D, Schmitz S, Bompas E, Dillies AF, Faivre S, Moxhon A, Duprez T, Guigay J. Phase II study of sunitinib in recurrent or metastatic squamous cell carcinoma of the head and neck: GORTEC 2006–01. J Clin Oncol 2010;28:21–28. [PubMed: 19917865]
78. Fury MG, Zahalsky A, Wong R, Venkatraman E, Lis E, Hann L, Aliff T, Gerald W, Fleisher M, Pfister DG. A phase II study of SU5416 in patients with advanced or recurrent head and neck cancers. Invest New Drugs 2007;25:165–172. [PubMed: 16983506]
79. Gerstner ER, Duda DG, di Tomaso E, Ryg PA, Loeffler JS, Sorensen AG, Ivy P, Jain RK, Batchelor TT. VEGF inhibitors in the treatment of cerebral edema in patients with brain cancer. Nat Rev Clin Oncol 2009;6:229–236. [PubMed: 19333229]
80. Zhang XM, Yu D, Zhang HL, Dai Y, Bi D, Liu Z, Prince MR, Li C. 3D dynamic contrast-enhanced MRI of rectal carcinoma at 3T: correlation with microvascular density and vascular endothelial growth factor markers of tumor angiogenesis. J Magn Reson Imaging 2008;27:1309–1316. [PubMed: 18504761]
81. Shiyan L, Pintong H, Zongmin W, Fuguang H, Zhiqiang Z, Yan Y, Cosgrove D. The relationship between enhanced intensity and microvessel density of gastric carcinoma using double contrast-enhanced ultrasonography. Ultrasound Med Biol 2009;35:1086–1091. [PubMed: 19419811]
82. Guo J, Higashi K, Ueda Y, Oguchi M, Takegami T, Toga H, Sakuma T, Yokota H, Katsuda S, Tonami H, Yamamoto I. Microvessel density: correlation with 18F-FDG uptake and prognostic impact in lung adenocarcinomas. J Nucl Med 2006;47:419–425. [PubMed: 16513610]
83. Lawrentschuk N, Poon AM, Foo SS, Putra LG, Murone C, Davis ID, Bolton DM, Scott AM. Assessing regional hypoxia in human renal tumours using 18F-fluoromisonidazole positron emission tomography. BJU Int 2005;96:540–546. [PubMed: 16104907]
84. Jain RK. Normalization of tumor vasculature: an emerging concept in antiangiogenic therapy. Science 2005;307:58–62. [PubMed: 15637262]
85. Oostendorp M, Post MJ, Backes WH. Vessel growth and function: depiction with contrast-enhanced MR imaging. Radiology 2009;251:317–335. [PubMed: 19401568]

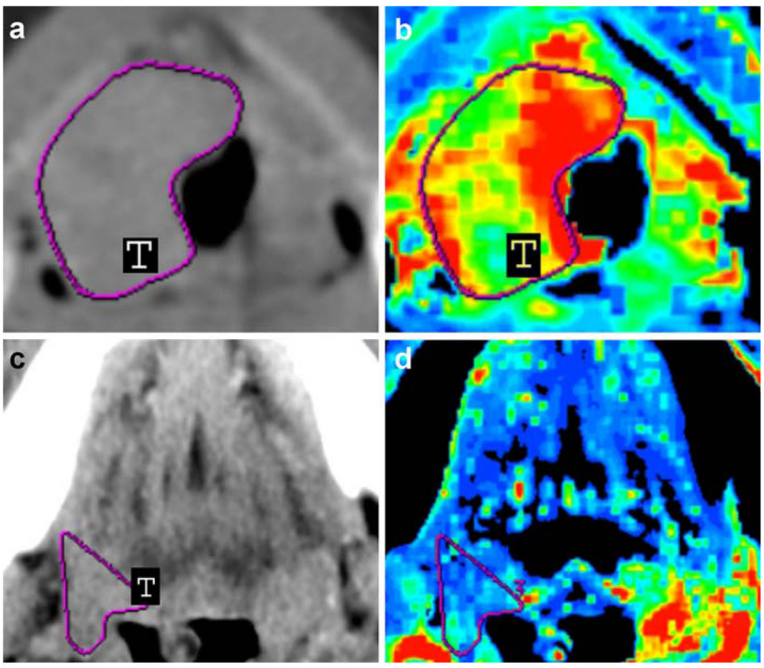

Fig. 1.

Contrast-enhanced neck CT scans (**a**, **c**) and CT perfusion maps (**b**, **d**) of a 45-year-old man with stage IV (*a–b*) and a 57-year-old woman with stage III (*c–d*) HNSCC in the base of the tongue. Solid tumor masses are indicated with T in (*a*, *c*). CT perfusion map (*b*) shows elevated blood flow (190.15 ml/100 g/min), which was confirmed by relative increased intratumoral MVD (47.2 vessels per square millimeter), whereas CT perfusion map (**d**) shows decreased blood flow (39.13 ml/100 g/min), which was confirmed by relative decreased intratumoral MVD (19.2 vessels per square millimeter). Reprinted with permission from [26]

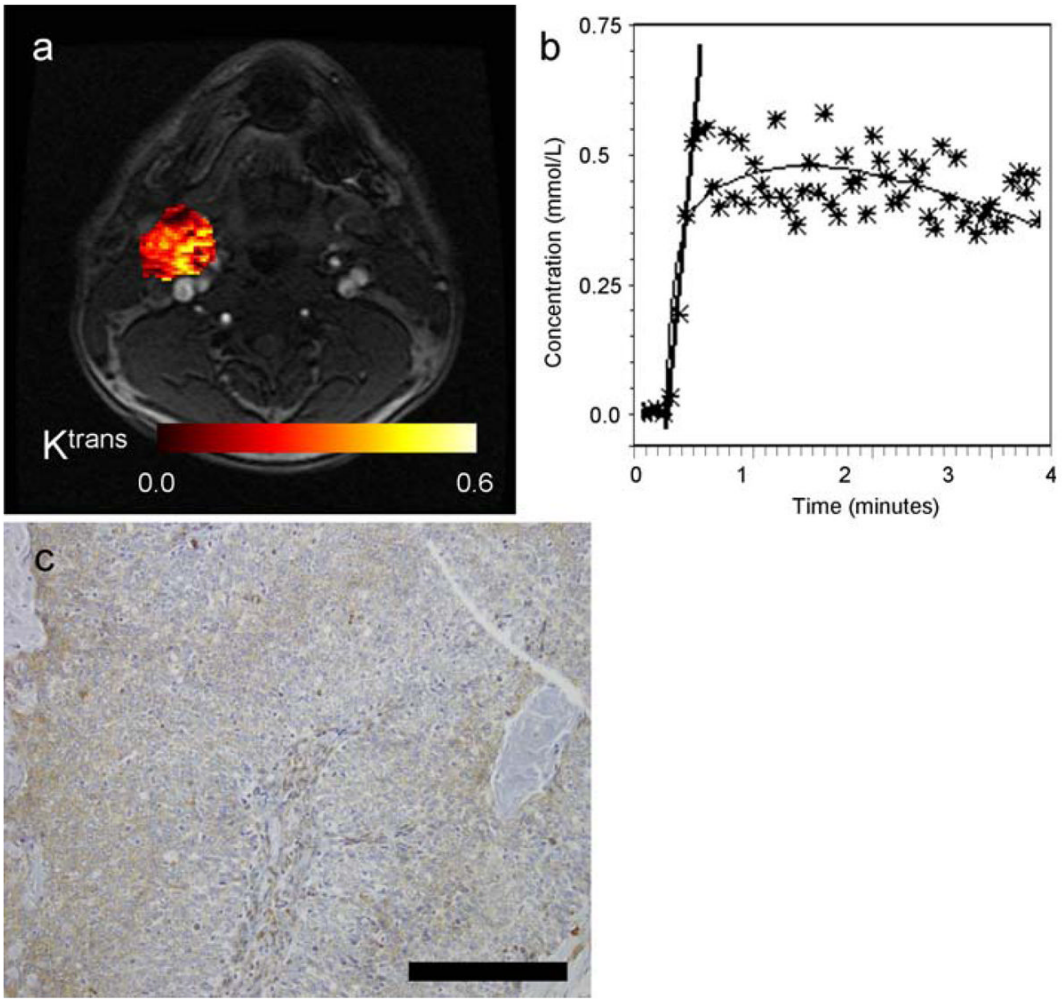

Fig. 2.

Images illustrating the left neck lymph node of a patient with HNSCC (male, 49 years old, primary cancer unknown). **a** Post-contrast axial MR image extracted from the DCE-MRI scan with the calculated parametric K^{trans} map of the node overlaid on the DCE-MR image. **b** DCE-MRI signal, converted into Gd-DTPA concentrations, as a function of acquisition time. The *stars* indicate the individual data points (averaged over the ROI), the *thin black line* is the fit, and the *thick black line* indicates the slope. **c** VEGF immunostaining of corresponding tumor surgical specimen, indicating high expression. *Black bar* indicates 0.2 mm

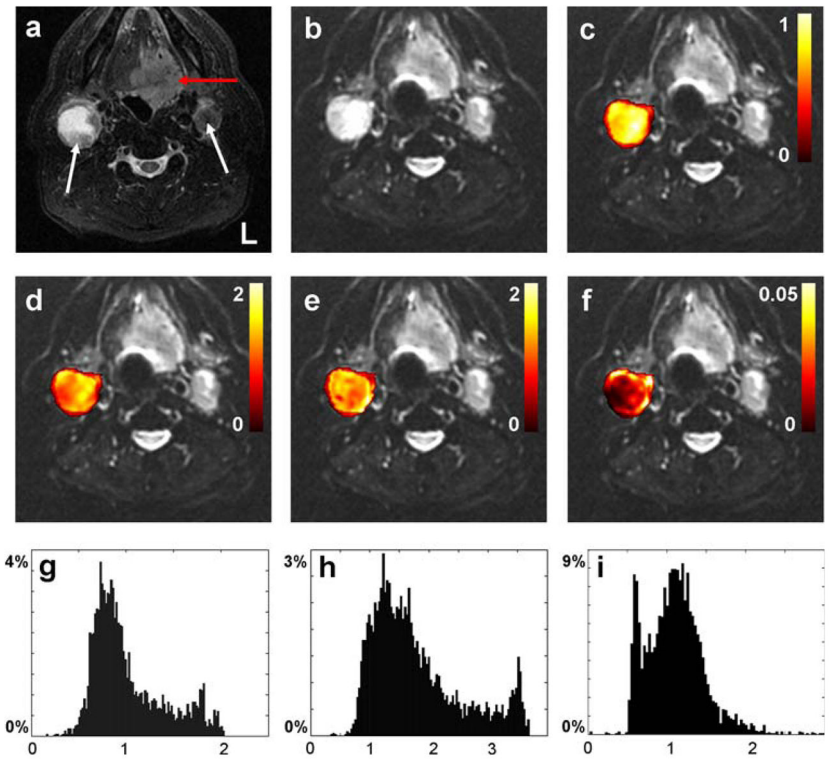

Fig. 3.

Axial MR images from the oral cavity of 60-year-old man diagnosed with HNSCC in the base of the tongue. **a** T2 short tau inversion recovery (STIR) image, **b** realigned mean $b = 0$ image. The *red* and *white arrows* in (*a*) indicate the primary tumor and metastatic nodes, respectively. Figures (**c**–**f**) display voxel-by-voxel calculation outcomes for the *right* node presented as mask overlays on the realigned mean $b = 0$ image. *Graphs* (**g**–**i**) display the corresponding histogram distribution plots of the measures from (**c**–**e**). **c, g** Apparent diffusion coefficient obtained from Gaussian monoexponential fitting (10^{-3} mm^2/s). **d**, **h** Apparent diffusion coefficient (10^{-3} mm^2/s), **e, i** apparent kurtosis coefficient (dimensionless), and **f** reduced χ^2 error estimate, all obtained from the non-Gaussian diffusional kurtosis analysis. Reprinted with permission from [41]

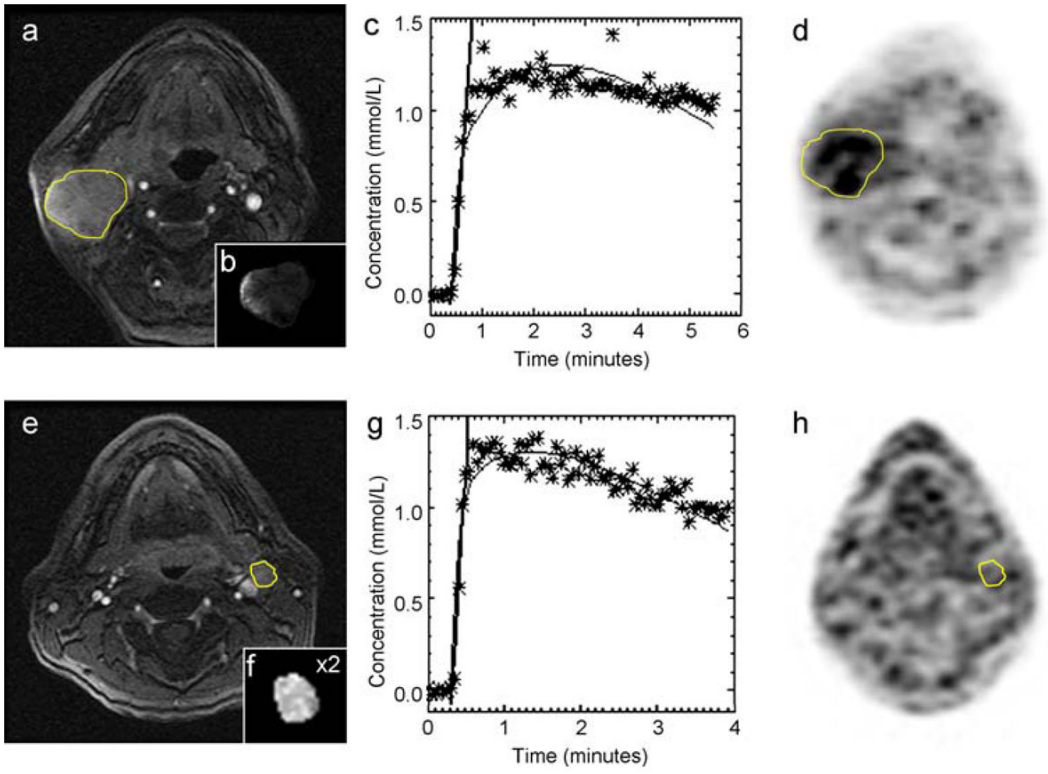

Fig. 4.

a–**d** MRI and ^{18}F-FMISO PET images illustrating the hypoxic right neck lymph node of a patient (male, 62 years old, primary tonsil cancer). **a** Shows the post-contrast multi-phase spoiled gradient echo. The node is outlined in *yellow*. The insert (**b**) in (**a**) displays the calculated parametric K^{trans} map of the node. In (**c**), the DCE-MRI signal (converted into Gd-DTPA concentrations) over the acquisition time is illustrated. The *stars* indicate the individual data points (averaged over the ROI), the *thin black line* is the fit, and the *thick black line* indicates the slope. Finally, in (**d**) the corresponding ^{18}F-FMISO image is shown, indicating ^{18}F-FMISO uptake in the node outlined in *yellow*. (**e**–**h**) MRI and ^{18}F-FMISO PET images illustrating the non-hypoxic left neck lymph node of a patient (male, 51 years old, primary tonsil cancer). Reprinted with permission from [62]

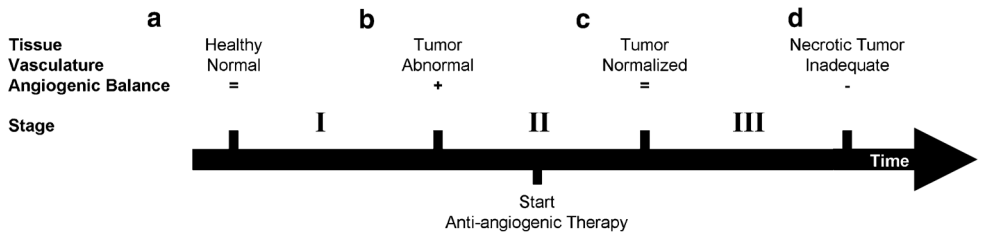

Fig. 5.

Schematic of changes in tumor vasculature during tumor formation and the course of anti-angiogenic therapy. **a** Healthy tissue has normal vasculature, which is composed of mature vessels and has an exact balance of pro- and anti-angiogenic molecules. **b** The activation of the angiogenic switch enables the tumor to engage surrounding blood vessels and promote formation of new vessels. The abnormal tumor vasculature provides the tumor with oxygen and nutrients, which facilitate more growth. **c** Administration of anti-angiogenic therapies prune immature vessels, which results in more normalized tumor vasculature (as proposed by Jain [84]). The resulting network is more effective for the transport of therapeutics and nutrients. **d** Rapid pruning of tumor vasculature reduces the integrity of vasculature network. The network is unable to facilitate tumor growth and could result in tumor dormancy, which is the ultimate goal of anti-angiogenic therapy. Figure conceptualized from [79] and [85]. Table 1 shows angiogenesis-related processes during the stages of tumor formation (I) and eradication (II–III), and best suited imaging modalities for their assessment

Table 1

Application of imaging modalities for monitoring angiogenesis-related processes in tumor formation and anti-angiogenic therapy

Process	Imaging modality	Stage		
		I	II	III
		Malignant transformation	Start anti-angiogenic therapy	Starvation of tumor
Angiogenesis	F-Galacto RGD-PET	+	−	−
Proliferation	FLT-PET, 1H-MRS (choline), 31P MRS (PME and PDE)	+	−	−
Vascularity	CT perfusion, DCE-MRI	+	−	−
Hypoxia	FMISO PET, 1H-MRS (lactate)	+	−	−
Blood flow	US	−	+	−
Perfusion	CT perfusion, DCE-MRI	−	+	−
Necrosis	DWI (ADC), MRI/CT	NA	NA	+
Growth in volume	MRI/CT	+	−	−
Biomarker upregulation[a]	Molecular imaging	±	±	±

The processes represent the overall characteristics of the tumor and do not take into account the intratumor heterogeneity +, positive effect; −, negative effect; NA, not applicable

[a]Due to the diversity of possible biomarkers for MI, the process can either be up- or down-regulated